Letter

Kink propagation and solute partitioning in an atomic monolayer on a substrate

Metehan Çam* and Seth Lichter†
Department of Mechanical Engineering, Northwestern University, Evanston, Illinois 60208, USA

Christopher G. Goedde‡
Department of Physics and Astrophysics, DePaul University, Chicago, Illinois 60614, USA

(Received 11 June 2021; accepted 29 July 2021; published 17 August 2021)

When a monolayer of Lennard-Jones atoms is driven by an external force over an atomically spaced lattice, the atoms do not move in the direction of the force. By considering monolayers containing a solvent and two different solutes, we show that the different atomic species follow distinct directions and so partition from one another and from the solvent. The strength of the driving force is chosen so that at any instant, most atoms are stationary while only a small fraction propagates as solitary waves. In this regime, the mean velocity of the layer is due to the nonzero contribution from merely a few atoms. We also present a simple theory, based on the probability that an atom in the monolayer will hop from one equilibrium location to the next, that explains the distinct directions of atomic migration.

DOI: 10.1103/PhysRevE.104.L022801

I. INTRODUCTION

When small particles move over a substrate, they do not follow the direction of the force. Rather, it is observed that the particle trajectories align with certain lattice directions of the substrate [1–10]. The trajectory direction is sensitive to the particle properties, encouraging potential applications to particle sorting and nanodevice assembly. Experimental studies have investigated the dynamical and directional behavior of micron- and nano-sized monolayers [1,6,10,11] as well as of micro- and nanofluidic systems [9,12] with the smallest particle size of about 20 nm [4].

To our knowledge, however, directionality of atomic-sized particles over atomically corrugated substrates has not been investigated. Studies of molecular motion in the vicinity of a substrate have the potential to advance our understanding of a range of phenomena including surface diffusion [13–15], fluid slip [16–18], molecular-level sorting [19,20], and lubrication [21].

In this Letter, we report on a numerical simulation of the dynamics of a monolayer of Lennard-Jones (LJ) atoms driven by an external force over a thermal solid substrate of simple cubical symmetry. In these simulations, we consider monolayers of pure solvent as well as solutions that contain solute atoms. We vary the direction of the applied force and investigate the directions that monolayer atoms follow and their dynamics. We show that for a dense monolayer that is commensurate with the substrate lattice, both solvent and solute atoms propagate in directions different from one another, resulting in the solute atoms partitioning from the solvent as a result of their particular energetic interaction with the substrate potential. We find that directionality can be understood after recognizing that at any instant, the dynamics of the monolayer is dominated by the motion of only a small fraction of mobile atoms.

While the mean properties of atomic monolayers have been studied [22–24], the motion of individual atoms in dense monolayers close to a surface has remained an open question [25]. We find that, at any instant, while most atoms reside close to their static equilibrium locations, there is a small fraction of peripatetic atoms that propagate. The sequential set of atoms set into motion constitute a disturbance that we refer to as a kink. The theoretical paradigm for motion of particles over a rigid periodic substrate is the Frenkel-Kontorova (FK) model [7,8,26–29]. We find that the propagation of a kink of discrete atoms over a substrate with a large activation energy is approximated by the sine-Gordon (sG) equation, which is the continuum version of the FK model. Kinks are shown to be localized with a well-defined width and a speed that agrees well with the speed of sG solitons. In our system they are also topological with each kink being annihilated or created pairwise with a vacancy. Finally, the kinks can preserve their form but are phase shifted by kink-vacancy interactions.

II. METHODOLOGY

We carry out nonequilibrium molecular dynamics simulations of monolayers of pure solvent LJ atoms as well as of solutions that contain solute atoms that differ in interaction strength from the solvent atoms, as shown in Fig. 1 [30]. The monolayer is driven over the substrate by applying an external force on all atoms in the monolayer. The temperature of the substrate T is maintained at 85 K by using a Langevin thermostat; solvent and solute atoms are not thermostatted. Nonbonded interactions are modelled by the LJ potential,

*metehancam2023@u.northwestern.edu
†s-lichter@northwestern.edu
‡cgoedde@depaul.edu

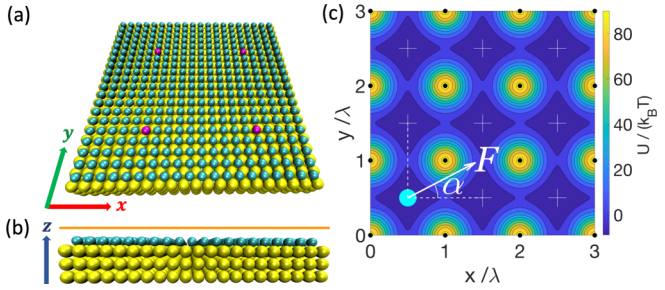

FIG. 1. (a) Snapshot showing the monolayer of solvent (cyan) and solute (magenta) atoms, which are initially located at the equilibrium locations of the LJ potential of the simple cubical lattice substrate (yellow). (b) Side view. Solid (orange) line indicates the upper limit of the restraining potential at $z = 2\sigma$ above the substrate (see text). (c) Substrate potential U normalized by the thermal energy k_BT as a function of x and y for a solvent atom at the mean height of the monolayer. Plus (white) markers indicate the equilibrium locations of the monolayer atoms over the substrate, while the horizontal and vertical (dashed) lines indicate low-energy corridors connecting neighboring equilibrium locations. Atoms in the monolayer are subject to an external driving force F applied at angle α.

$U = 4\epsilon[(\sigma/r)^{12} - (\sigma/r)^6]$, which provides a simple model of atomic interaction, with only an energy parameter ϵ and a length parameter σ. Atomic masses are 14 u for the solvent and solute atoms and 197 u for the substrate atoms.

Table I shows the LJ energy parameters of the four types of atoms that are present in the numerical simulations. The length parameter is the same for solvent and solute atoms so that they both are commensurate with the substrate lattice. Two types of solute atoms were used, which we refer to as solute A and solute B. Both solute species have larger LJ energy parameters than the solvent, making them harder to move from their equilibrium locations in the substrate potential.

Table I also shows U_0, the minimum amplitude of the substrate potential for each of the three types of monolayer atoms. Here U_0 is found from the difference between the potential energy minimum half-way between two equilibrium locations and the LJ energy at the equilibrium location.

The solid substrate consists of three 40×40 layers of atoms that are tethered to their cubical lattice positions with a lattice spacing of $\lambda = 2^{1/6}\sigma = 0.298$ nm by linear springs with a stiffness $k = 46.8$ N/m. Periodic boundary conditions are implemented in x and y directions of the square cell, which has dimensions $L_x = L_y = 40\,\lambda$.

TABLE I. The Lennard-Jones energy parameter, ϵ, of the four types of atoms in the simulation, and the minimum amplitude of the LJ potential, U_0, experienced by the atoms in monolayer. All atoms have the same LJ length parameter of $\sigma = 0.266$ nm.

Atom type	ϵ/k_BT	U_0/k_BT
Solvent	0.553	2.321
Solute A	2.212	3.844
Solute B	6.227	5.795
Substrate	6.227	–

To keep the solvent and solute atoms constrained to a monolayer, motion in the z direction normal to the substrate is restrained by a repulsive LJ potential, $U_{\rm rep}(z) = 4\,\epsilon_{\rm rep}[\sigma/(2\sigma - z)]^{12}$, where z is measured from the equilibrium height of the uppermost layer of the substrate and $\epsilon_{\rm rep}/k_BT = 1.856$. This restraining potential places an upper limit of $z_{\rm max} = 2\sigma$ on the vertical motion of the atoms in the monolayer. In practice, the range of vertical motion of the atoms in the monolayer is much smaller, with the mean vertical position of the monolayer atoms ranging from 0.79σ to 0.91σ above the upper layer of the substrate.

Both the solvent and solute atoms are initially located at the minima of the substrate potential energy landscape, as depicted in Fig. 1. The external force applied to all atoms in the monolayer is specified by its magnitude F and direction α. The applied force is chosen to be of sufficiently small magnitude so that only some atoms are propagating at any time. In this regime, most atoms in the monolayer vibrate about their equilibrium location. Occasionally, however, a monolayer atom will "hop" in either the x or y direction, creating a defect in the monolayer in which one equilibrium cell is doubly occupied, and one is vacant. We refer to the doubly occupied equilibrium location as a kink. The kink then propagates through the monolayer as neighboring atoms hop one by one. Because the probability of initiating a hop depends on the strength and direction of the external force, the strength of the external force at each angle was chosen so that the rate of hopping was comparable at all angles, yielding an applied force between 20.1 and 23.2 pN over the entire range of $0^\circ \leqslant \alpha \leqslant 45^\circ$.

The direction of atomic migration was analyzed through simulations with a duration of 140 ns and using a 5 ps sampling rate. However, in order to resolve the individual propagation of kinks and vacancies in the monolayer, femtosecond resolution in atomic positions is needed because the individual atomic hops between equilibrium locations take less than a picosecond. Therefore, simulations to resolve the kink and vacancy dynamics have a duration of 2.5 ns and a sampling rate of 10 fs.

III. ATOMIC MIGRATION RESULTS

We define a hop as the displacement of an atom from one equilibrium position to a neighboring equilibrium position, and an atomic trajectory as the path a single atom takes through the monolayer via a sequence of individual hops. Figure 2 shows the atomic trajectories of a single solvent atom (blue) and two individual solute atoms (red for solute A and green for solute B) for a forcing angle of $\alpha = 27.5^\circ$ over a 13-ns segment of a 140-ns simulation. Since the solvent has the smallest LJ energy parameter, these atoms move the most freely over the surface and undergo the largest displacement. The two solute atoms, with larger LJ energies, do not hop as frequently and have a smaller net displacement. As can be seen from the figure, most hops occur in either the x or y direction, as the hopping atoms follow the low-energy corridors in the substrate potential. At this angle of the driving force, hops in the x direction occur much more frequently than hops in the y direction, leading to atomic migration angles that differ from the angle of the driving force. Crucially, the migration angle

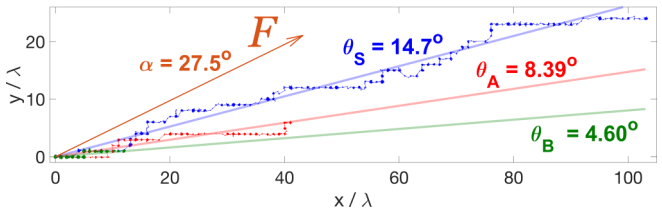

FIG. 2. Representative trajectories following individual solvent and solute atoms over a 13-ns time interval for a forcing angle of $\alpha = 27.5^\circ$ (orange arrow). The trajectory of a typical solvent atom is shown in blue; trajectories for typical solute A and solute B atoms are shown in red and green, respectively. The migration angles for the center of mass of the three species of atoms are indicated by the solid lines at angles of 14.7° for the solvent and 8.39° and 4.60° for the solutes. Coordinates have been translated to a common origin and normalized by the lattice constant λ.

for the center-of-mass motion of each atomic species (shown as the straight lines in Fig. 2) are different from the driving angle α and from each other. Thus, we see that neither the solvent nor the solute migrate in the direction of the external forcing.

Figure 3 shows the angle of center-of-mass migration for the solvent and each of the solutes as the direction of the applied force is varied over the range $0^\circ \leqslant \alpha \leqslant 45^\circ$. In general, the angle of center-of-mass migration differs significantly from the angle of the driving force. (At 0° and 45°, the angle of center-of-mass migration and the angle of the driving force must be equal due to symmetry.) The difference is largest at a driving angle of 27.5° and increases with increasing LJ energy, so that solute B shows the largest deviation in migration angle.

The trajectories in Fig. 2 follow individual atoms. Alternatively, we track the disturbance created as atoms leave their equilibrium locations. When an atom hops spontaneously, it leaves behind a vacant equilibrium location and moves into an already-occupied equilibrium location. The original occupant of the doubly occupied site is then dislodged, and it then moves forward, resulting in a sequence of hopping atoms and generating the trajectory for the kink. This trajectory will continue until the kink recombines with a vacancy. Since the kink trajectories consist of sequences of hops of neighboring atoms, they tend to follow similar patterns as the trajectories of individual atoms, with the kinks traveling along the low-energy corridors in the LJ potential, as shown in Fig. 4(a).

The monolayer is initialized with the number of monolayer atoms equal to the number of equilibrium sites. During a typical simulation, at most 2.5% of the monolayer atoms are participating in the kinks while all other monolayer atoms fluctuate around their equilibrium sites. While the number of kinks varies in time, Fig. 4(b), they are found to be topologically stable, where the instantaneous number of kinks is always equal to the number of vacancies. Since the kink convects atoms as it propagates, it is the small population of

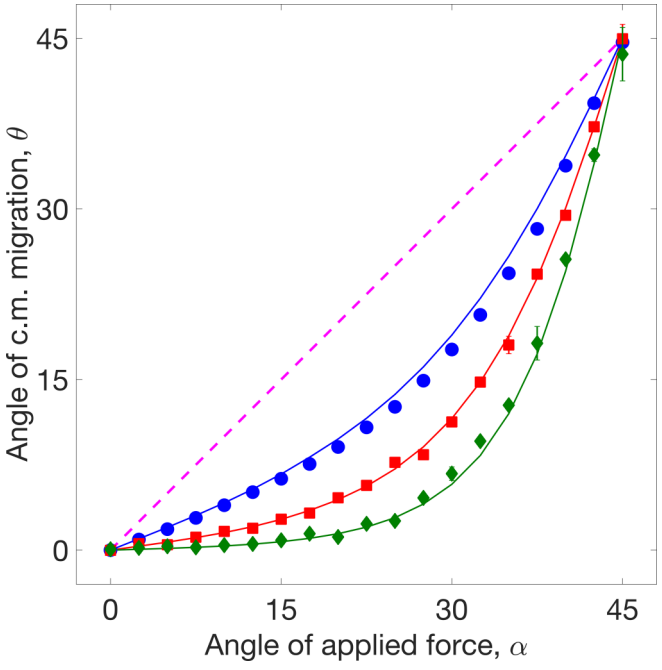

FIG. 3. The migration angle of the center of mass (c.m.) for atoms in the monolayer, θ, as a function of the angle of the applied force, α. Solvent: Blue circles; Solute A: Red squares; Solute B: Green diamonds. The solid lines are the theoretical predictions for the solvent, Eq. (2), and the solute atoms, Eq. (3). Error bars indicate the standard deviation of the mean migration angle at each driving angle. In only a few cases are the error bars larger than the symbols on the figure.

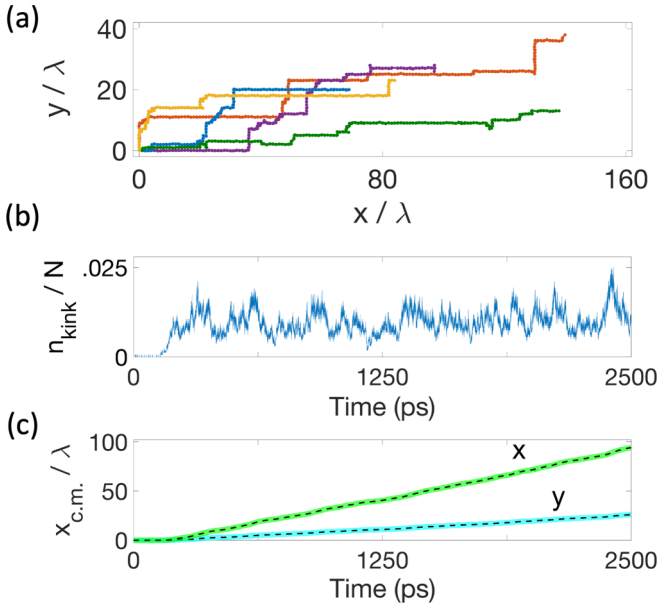

FIG. 4. (a) Five representative kink trajectories at angle $\alpha = 27.5^\circ$. Coordinates have been translated to a common origin and normalized by the lattice constant λ. (b) The number of kinks n_{kink} normalized by the number of atoms in the monolayer, N, as a function of time for an applied force at angle $\alpha = 27.5^\circ$. (c) The x position (green line) and y position (cyan line) of the center of mass (c.m.) of the monolayer, obtained by averaging the x and y positions of all N monolayer atoms, matches perfectly at all times with results from the mass convected by the kinks and vacancies (black dashed lines).

kinks and vacancies that results in the center of mass of the monolayer moving over the substrate, Fig. 4(c).

To explain the observed deviation between the angle of forcing α and the observed migration angle θ of the center of mass, we formulate a model based on the differential probability of hopping in the x or y direction. We assume that the rate of hopping is determined by the work done on the atom that hops. We take the mean angle θ to be given by

$$\tan\theta = \frac{\text{probability of hop in } y \text{ direction}}{\text{probability of hop in } x \text{ direction}}. \tag{1}$$

We assume that the probabilities of hopping in the x and y directions are proportional to their Boltzmann factors. For solvent atoms this can be written in terms of the work done by the external force (accounting for hops in both the positive and negative directions) as

$$\tan\theta = \frac{\sinh\left[\beta F(\lambda/2)\sin\alpha\right]}{\sinh\left[\beta F(\lambda/2)\cos\alpha\right]}. \tag{2}$$

Here the work done is calculated using the appropriate (x or y) component of the driving force when moving a solvent atom by a distance of $\lambda/2$. Equation (2) constitutes a prediction for the migration angle for solvent atom. If we use the force values from the simulation for the magnitude of the driving force F, then we obtain the solid blue line shown in Fig. 3, which is in excellent agreement with the observed migration angle for the solvent.

Because the solute atoms have larger LJ energy parameters, they do not hop spontaneously, and the work required to cause a solute atom to hop is greater than that supplied by the external forcing. As a result, solute atoms only hop due to a collision from an incoming kink. The additional work ΔU required for a solute atom to hop can be found from the difference in the potential that the solute atoms experience compared to the solvent atoms. So, from Table I, ΔU is the difference in value of U_0 for a solute from the U_0 of the solvent. For the solute atoms, Eq. (2) then becomes

$$\tan\theta = \frac{\sinh\left\{\beta[\Delta U + F(\lambda/2)]\sin\alpha\right\}}{\sinh\left\{\beta[\Delta U + F(\lambda/2)]\cos\alpha\right\}}. \tag{3}$$

For solute A this difference is $\Delta U_A/k_BT = 1.523$, and for solute B it is $\Delta U_B/k_BT = 3.474$. The corresponding theoretical predictions are shown as the red and green solid lines in Fig. 3, again in excellent agreement to the observed migration angles. In both the high- and low-temperature limits, Eq. (3) predicts that the migration angles of all species go to a common limit. Hence, there is a range of intermediate temperatures which optimize the separation of different species.

IV. KINK DYNAMICS

Key aspects of the kink dynamics on this discrete lattice can be described by the behavior of solitons in the continuum sine-Gordon equation. Neglecting the discreteness effects in the standard FK model, the equation of motion reduces to the sine-Gordon (sG) equation [31],

$$u_{tt} - u_{xx} + \sin u = 0. \tag{4}$$

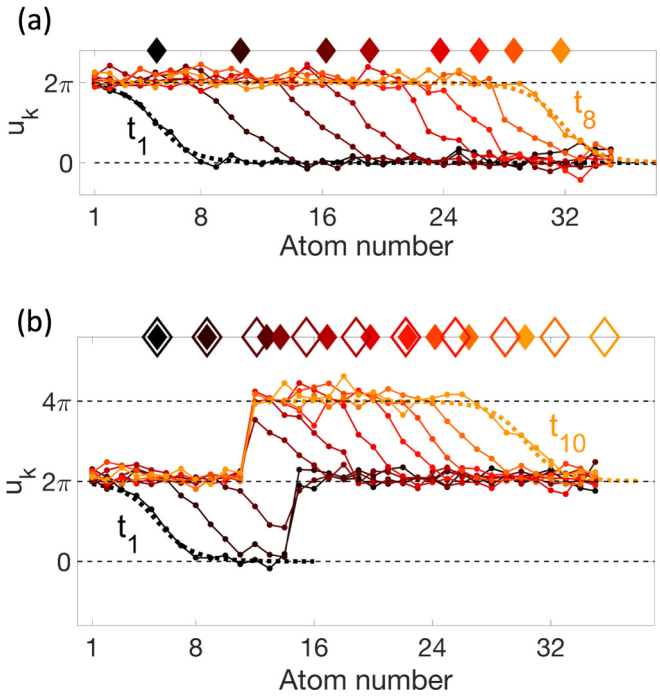

FIG. 5. Kink profiles showing the x positions of 35 contiguous atoms in the monolayer with respect to their initial substrate equilibrium sites. (a) A single traveling kink shown at intervals of 0.5 ps (color coded). Filled diamonds at the top indicate the location of the center of the kink at each time shown. (b) A kink passing through a vacancy, shown every 0.4 ps (color coded). Filled diamonds indicate the location of the kink center; open diamonds indicate the center of constant-velocity kink (see text). In both panels, dashed lines at the initial and final frames depict the sG profiles with $\gamma = 1.26$.

Topological solitons appear as one of the solutions to the sG equation,

$$u(x,t) = 4\tan^{-1}\exp\left\{-\gamma[x - x_0 - v(t - t_0)]\right\}, \tag{5}$$

$$\gamma = 1/\sqrt{1 - v^2}, \tag{6}$$

where v is the velocity of the kink measured in units of sound velocity c and x_0 is the location of the center of the kink at time t_0. The sound velocity $c = 4052$ m/s was found from the oscillation frequency of a pure-solvent monolayer with zero external forcing. To compare the sG results to our observations, we evaluate the continuum results at discrete points k and divide the displacement by $\lambda/2\pi$, yielding u_k, the nondimensional x displacement of the atoms, as described by Eq. (5). With this normalization, the equilibrium spacing of the atoms in the monolayer is 2π.

Figure 5(a) shows eight profiles of a kink during a 4-ps interval as it propagates through the monolayer. The width, $1/\gamma$, and position, x_0, of the kink can be determined by the slope and intercept of a straight line fit to the inverse of Eq. (5). The snapshots shown here are for a kink that has an average velocity of $v = 0.61$ and an average width corresponding to $\gamma = 1.26$. (For comparison, the fitted sG profile from Eq. (5) is shown as the dashed line at the first and last times.) While the observed profile fluctuates as the kink propagates, its overall shape is preserved. Similarly, the instantaneous velocity of

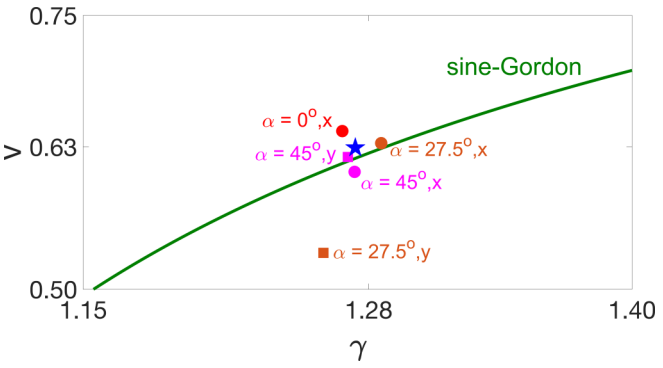

FIG. 6. Relationship between the inverse width γ and velocity v averaged over a large sample of kinks at forcing directions $\alpha = 0°$, 27.5°, and 45° in a pure solvent monolayer. Kinks propagating in the x and y directions are plotted separately. The blue star shows the mean of all the sampled kinks: ($\gamma = 1.27$, $v = 0.63$). The green line indicates the prediction of the sG equation, Eq. (6).

the kink fluctuates, as indicated by the irregular spacing of the filled diamonds at the top of the figure, which mark the location of the center of the kink for each snapshot.

Figure 5(b) shows the collision of a kink with a vacancy (which is initially located at atom number 15) over a 4-ps interval. During its interaction with the vacancy, the form of the kink changes markedly from its sG form. However, the kink that re-emerges from the interaction has the same average width (corresponding to $\gamma = 1.26$) and speed ($v = 0.66$) as the kink that entered into the interaction with the vacancy.

The emergent kink is, however, delayed by its interaction with the vacancy; its position, shown by the filled diamonds, lags behind where it would have been (open diamonds) had the interaction not occurred. As a result of the collision, the kink undergoes a time delay of 0.67 ps and position delay of 5.4λ. This behavior is remarkably similar to the interaction of a sG soliton and a sG antisoliton: The shape of the monolayer kink remains invariant through the interaction and the interaction introduces a phase shift in the position of the kink.

To make a quantitative comparison of the observed kinks with sG solitons, we measured the velocity and width of 1400 kinks at high resolution, sampling at intervals of 10 fs. We separated the kinks into sets based on the forcing angles of $\alpha = 0°$, 27.5°, and 45° and their direction of travel, either in the x or y direction. Each individual set has an average velocity and width which consistently agrees with the prediction of sG equation. The correspondence between velocity and width for the individual sets is shown in Fig. 6. While most of the data in Fig. 6 lies close to the theoretical sG curve, the data point for y-moving kinks at a forcing angle of $\alpha = 27.5°$ is an outlier, possibly because this data set has, by far, the fewest (85) samples. The average velocity of all kinks over all samples is found to be $v = 0.63$, and the average value of γ is found to be 1.27. These values are shown as the blue star in Fig. 6 and are in very good agreement with the sG prediction given by Eq. (6) of $\gamma(v = 0.63) = 1.29$.

V. DISCUSSION AND CONCLUSIONS

We observe that when forced across an atomic substrate, atoms do not follow the direction of the external force, but that the center-of-mass motion of different species of atoms follow distinct directions according to the strength of their interaction with the substrate. We present a simple theory, based on the differential probability of atomic hops to nearby substrate equilibrium sites that explains the observed distinct migration angles.

We also observe that, at any instant, while most atoms fluctuate near their equilibrium positions, there is a small fraction of peripatetic atoms. These atoms leave their equilibrium locations, creating vacancies in the monolayer, and collide with other atoms, generating a sequence of adjacent atoms hopping from one equilibrium site to another in a propagating disturbance that we refer to as a kink. We show that the motion of the monolayer over the substrate is due to the sum of the individual propagation of kinks and their associated vacancies.

Remarkably, the kinks on this discrete substrate are observed to possess properties of continuum sG solitons: (i) they are localized, with a well-defined width; (ii) their profile is consistent with that of sG solitons; (iii) kinks are topological, appearing or disappearing pairwise with vacancies; (iv) kink velocity is in good agreement with the prediction of sG equation; and (v) on emerging from an interaction with a vacancy, a kink maintains its profile but is delayed.

Our Lennard-Jones simulations and theoretical model demonstrate how individual atoms move over an atomic substrate while they are being separated based on their interaction strength. Directionality of atomic trajectories in monolayers may provide a means for molecular sorting and inspire the design of new separation technologies. In this study, we only consider the separation of solutes from solvents based on the energy parameters of the atoms. Future studies will address separation based on the length parameter σ of the atoms. In this study, we only consider a substrate with square symmetry although we look forward to investigating substrates with other structure, including the interesting hexagonal symmetry of graphene. These future studies with more varied and realistic models and materials would indicate the robustness, scope and feasibility of molecular sorting over a substrate. In summary, we report on a new fundamental phenomena of kink propagation in atomic monolayers, whose generality and potential technological applicability continue to be investigated.

ACKNOWLEDGMENTS

This research was supported in part through the computational resources and staff contributions provided for the Quest high performance computing facility at Northwestern University which is jointly supported by the Office of the Provost, the Office for Research, and Northwestern University Information Technology.

[1] X. Cao, E. Panizon, A. Vanossi, N. Manini, and C. Bechinger, Nat. Phys. **15**, 776 (2019).
[2] J. Koplik and G. Drazer, Phys. Fluids **22**, 052005 (2010).
[3] C. Reichhardt and C. O. Reichhardt, Rep. Prog. Phys. **80**, 026501 (2016).
[4] B. H. Wunsch, J. T. Smith, S. M. Gifford, C. Wang, M. Brink, R. L. Bruce, R. H. Austin, G. Stolovitzky, and Y. Astier, Nat. Nanotechnol. **11**, 936 (2016).
[5] J. Frechette and G. Drazer, J. Fluid Mech. **627**, 379 (2009).
[6] R. L. Stoop, A. V. Straube, T. H. Johansen, and P. Tierno, Phys. Rev. Lett. **124**, 058002 (2020).
[7] C.-L. Wang, W.-S. Duan, X.-R. Hong, and J.-M. Chen, Appl. Phys. Lett. **93**, 153116 (2008).
[8] Y. Yang, W.-S. Duan, J.-M. Chen, L. Yang, J. Tekić, Z.-G. Shao, and C.-L. Wang, Phys. Rev. E **82**, 051119 (2010).
[9] K. Loutherback, J. Puchalla, R. H. Austin, and J. C. Sturm, Phys. Rev. Lett. **102**, 045301 (2009).
[10] T. Bohlein and C. Bechinger, Phys. Rev. Lett. **109**, 058301 (2012).
[11] T. Brazda, A. Silva, N. Manini, A. Vanossi, R. Guerra, E. Tosatti, and C. Bechinger, Phys. Rev. X **8**, 011050 (2018).
[12] L. R. Huang, E. C. Cox, R. H. Austin, and J. C. Sturm, Science **304**, 987 (2004).
[13] D. Wang, H. Wu, and D. K. Schwartz, Phys. Rev. Lett. **119**, 268001 (2017).
[14] R. Walder, N. Nelson, and D. K. Schwartz, Phys. Rev. Lett. **107**, 156102 (2011).
[15] M. J. Skaug, A. M. Lacasta, L. Ramirez-Piscina, J. M. Sancho, K. Lindenberg, and D. K. Schwartz, Soft Matter **10**, 753 (2014).
[16] A. Martini, A. Roxin, R. Q. Snurr, Q. Wang, and S. Lichter, J. Fluid Mech. **600**, 257 (2008).
[17] S. Lichter, A. Roxin, and S. Mandre, Phys. Rev. Lett. **93**, 086001 (2004).
[18] J.-L. Barrat and L. Bocquet, Faraday Discuss. **112**, 119 (1999).
[19] H. Li, J. Francisco, and X. Zeng, Proc. Natl. Acad. Sci. USA **112**, 10851 (2015).
[20] M. Heiranian, A. Barati Farimani, and N. Aluru, Nat. Commun. **6**, 8616 (2015).
[21] A. Martini, Y. Liu, R. Snurr, and Q. Wang, Tribol. Lett. **21**, 217 (2006).
[22] M. Cieplak, E. D. Smith, and M. O. Robbins, Science **265**, 1209 (1994).
[23] G. He, M. H. Müser, and M. O. Robbins, Science **284**, 1650 (1999).
[24] C. Lee, Q. Li, W. Kalb, X.-Z. Liu, H. Berger, R. W. Carpick, and J. Hone, Science **328**, 76 (2010).
[25] A.-K. Henß, S. Sakong, P. K. Messer, J. Wiechers, R. Schuster, D. C. Lamb, A. Groß, and J. Wintterlin, Science **363**, 715 (2019).
[26] O. M. Braun, M. V. Paliy, J. Röder, and A. R. Bishop, Phys. Rev. E **63**, 036129 (2001).
[27] O. M. Braun, T. Dauxois, M. V. Paliy, and M. Peyrard, Phys. Rev. Lett. **78**, 1295 (1997).
[28] Y. N. Gornostyrev, M. I. Katsnelson, A. V. Kravtsov, and A. V. Trefilov, Phys. Rev. B **60**, 1013 (1999).
[29] Y. N. Gornostyrev, M. I. Katsnelson, A. V. Kravtsov, and A. V. Trefilov, Phys. Rev. E **66**, 027201 (2002).
[30] J. C. Phillips, D. J. Hardy, J. D. Maia, J. E. Stone, J. V. Ribeiro, R. C. Bernardi, R. Buch, G. Fiorin, J. Hénin, W. Jiang *et al.*, J. Chem. Phys. **153**, 044130 (2020).
[31] O. M. Braun and Y. S. Kivshar, Phys. Rep. **306**, 1 (1998).